Journal of Molecular Catalysis A: Chemical 338 (2011) 84–91

Contents lists available at ScienceDirect

Journal of Molecular Catalysis A: Chemical

journal homepage: www.elsevier.com/locate/molcata

Heterogeneous photocatalysis of a dye solution using supported TiO_2 nanoparticles combined with homogeneous photoelectrochemical process: Molecular degradation products

A.R. Khataee*, M. Zarei, R. Ordikhani-Seyedlar

Department of Applied Chemistry, Faculty of Chemistry, University of Tabriz, Tabriz, Iran

ARTICLE INFO

Article history:
Received 14 October 2010
Received in revised form 16 January 2011
Accepted 25 January 2011
Available online 25 February 2011

Keywords:
TiO_2 nanoparticles
Carbon nanotube
Experimental design
Photodegradation
TOC

ABSTRACT

Treatment of a dye solution containing C.I. Basic Red 46 (BR46) by homogeneous photoelectro-Fenton (PEF) combined with heterogeneous photocatalytic process was studied. The investigated photocatalyst was TiO_2 nanoparticles (Degussa P-25) immobilized on glass plates. Carbon nanotube-polytetrafluoroethylene (CNT-PTFE) electrode was used as cathode. Response surface methodology (RSM) was employed to assess individual and interactive effects of the four key factors (initial amount of Fe(III), initial concentration of the dye, reaction time and applied current) in PEF/UV/TiO_2 process. Analysis of variance (ANOVA) showed a high coefficient of determination value (R^2 = 0.935) and satisfactory prediction second-order regression. Graphical response surface and contour plots were used to locate the optimum point. The optimum initial amount of Fe(III), initial dye concentration, reaction time and applied current were found to be 0.1 mM, 15 mg/L, 35 min and 300 mA, respectively. The observed experimental response was 88.89 of decolorization efficiency in optimum conditions of variables. The total organic carbon (TOC) measurements showed 99.2% mineralization of 15 mg/L dye at 6 h using PEF/UV/TiO_2 process. GC–MS analysis verified the identity of intermediates. The electrical energy consumption for the photo-electrochemical process was evaluated.

1. Introduction

Azo dyes are used extensively in textile dyeing and finishing operations and contribute to the pollution problems associated with disposal of a considerable amount of wastewater containing residual dyes [1]. Dyes present in wastewater are of particular environmental concern since they not only give an undesirable color to the waters but also in some cases are themselves harmful compounds and can originate dangerous byproducts through oxidation, hydrolysis, or other chemical reactions taking place in the waste phase [2].

So, there is a need to develop effective methods for the degradation of such organic pollutants, either to less harmful compounds or, more desirable, to their complete mineralization. Various technologies have been developed for environmental pollutants remediation [3–5]. In recent years indirect electrooxidation methods with hydrogen peroxide electrogeneration, such as electro-Fenton (EF) and photoelectro-Fenton (PEF) reactions, are being developed for the treatment of toxic organic pollutants in waters [3–11]. In these techniques, H_2O_2 is continuously supplied to the contaminated solution from the two-electron reduction of O_2 (Eq. (1)) usually at carbon-felt [7–9] and carbon-polytetrafluoroethylene (PTFE) O_2-diffusion [10–13] cathodes.

$$O_2 + 2H^+ + 2e^- \rightarrow H_2O_2 \quad (1)$$

In acidic aqueous medium the oxidation power will be enhanced by addition of Fe(II) or Fe(III) ions to the solution that allows the production of a very reactive one-electron oxidizing agent hydroxyl radical ($OH^\bullet$) from the well-known Fenton reaction (Eq. (2)) [6,14].

$$Fe(II) + H_2O_2 + H^+ \rightarrow Fe(III) + OH^\bullet + H_2O \quad (2)$$

Soluble Fe(III) can be reduced to Fe(II) through reaction (3) on cathode:

$$Fe(III) + e^- \rightarrow Fe(II) \quad (3)$$

The mineralization process can be accelerated using the PEF method, where the solution treated under EF conditions is exposed to an UV light. The photocatalytic action of this irradiation is complex and its main effects can be related to: (i) the photolysis of $Fe(OH)^{2+}$, which is the predominant Fe(III) species at pH 3.0, regenerating greater amount of Fe(II) and producing more quantity of

* Corresponding author. Tel.: +98 411 3393165; fax: +98 411 3340191.
E-mail addresses: a_khataee@tabrizu.ac.ir, ar_khataee@yahoo.com (A.R. Khataee), Mzarei@tabrizu.ac.ir (M. Zarei), ramin_ordikhani2@yahoo.com (R. Ordikhani-Seyedlar).

1381-1169/$ – see front matter © 2011 Elsevier B.V. All rights reserved.
doi:10.1016/j.molcata.2011.01.028

$OH^{\bullet}$ via photo-Fenton reaction (Eq. (4)) [15–17]:

$$[Fe(OH)]^{2+} + h\upsilon \rightarrow Fe(II) + OH^{\bullet} \quad (4)$$

and (ii) the photodecomposition of complexes of Fe(III) with generated carboxylic acids, e.g., oxalic acid. That is, at acidic pH, oxalic acids behave as photo-active complexes in the presence of ferric ions which undergo photo-decarboxylation reaction (Eq. (5)) [18]:

$$Fe(III)(RCO_2)^{2+} + h\upsilon \rightarrow Fe(II) + CO_2 + R^{\bullet} \quad (5)$$

On the other hand, heterogeneous photocatalysis through illumination of UV on semiconductor surface is an attractive advanced oxidation process. TiO_2 is a semiconductor and when it is illuminated with the light of $\lambda < 390$ nm, electrons are promoted from the valence band to the conduction band to give electron–hole pairs through reaction (6) [19,20]:

$$TiO_2 + h\upsilon (\lambda < 390\,nm) \rightarrow e^- + h^+ \quad (6)$$

The valence band (h^+) potential is positive enough to generate hydroxyl radicals at the surface of TiO_2 and the conduction band (e^-) potential is negative enough to reduce molecular oxygen as shown in Eqs. (7)–(11):

$$e^- + O_{2(ads)} \rightarrow {}^{\bullet}O_{2(ads)}{}^- \quad (7)$$

$$e^- + H_{(ads)}{}^+ \rightarrow {}^{\bullet}H_{(ads)} \quad (8)$$

$${}^{\bullet}O_{2(ads)}{}^- + H^+ \rightarrow HOO^{\bullet} \quad (9)$$

$$2HOO^{\bullet} \rightarrow H_2O_2 + O_2 \quad (10)$$

$$H_2O_2 + {}^{\bullet}O_{2(ads)}{}^- \rightarrow {}^{\bullet}OH + OH^- + O_2 \quad (11)$$

The hydroxyl radical is a powerful oxidizing agent and attacks organic matters present at or near the surface of TiO_2. It causes, ultimately, complete decomposition of toxic and bioresistant compounds into harmless species (CO_2, H_2O, etc.) [20,5,21].

BR46 is a dark red powder dye used in wool, silk, acrylic and polyester textile printing (sweaters, shirts, socks, etc.). Therefore, BR46 can be found in the effluents of the producing these matters. In this work, we have studied the removal of BR46 as a model dye from aqueous solutions using the process of PEF/UV/supported TiO_2 nanoparticles with CNT-PTFE electrode as cathode. We have also used response surface methodology to study the influence of experimental parameters on the decolorization efficiency of BR46 by PEF/UV/TiO_2 process. The color removal efficiency was selected as the response for optimization and the functional relationship between the response and the most significant independent variables (factors) was established by means of experimental design. Optimization of experimental parameters is usually assessed by systematic variation of one parameter while the others are maintained constant. This approach is unable to predict the optimized conditions of the process. In this respect, experimental designs are appropriate tools for process optimization. In fact, the experimental design allows considerable reduction of experiments number and a rapid interpretation. In the experimental design, it is possible to study a large number of factors and to detect the possible interactions between them. All the parameters are simultaneously applied in order to calculate their relative effect [22].

2. Materials and methods

2.1. Chemicals

C.I. Basic Red 46 (BR46) was purchased from Shimi Boyakhsaz Co., Iran (λ_{max} 530 nm, M_w 357.5 g/mol, purity > 95%) (Fig. 1a). Sulfuric acid, anhydrous sodium sulfate, N,O-bis(trimethylsilyl)acetamide and Iron(III) chloride were obtained from Merck Co. (Germany). The other chemicals used in this study

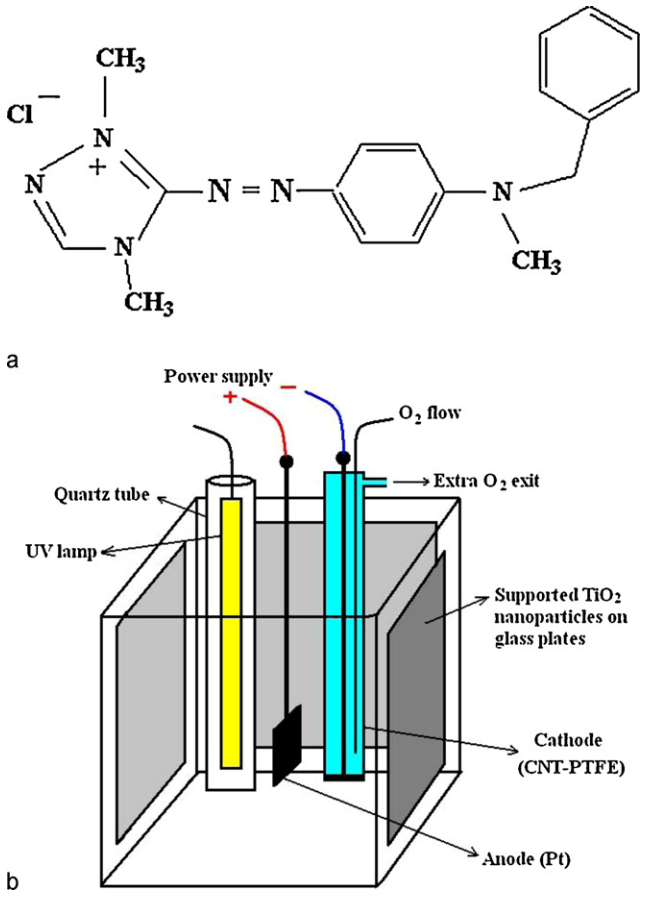

Fig. 1. (a) Chemical structure of C.I. Basic Red 46 (BR46), and (b) schematic diagram of the used electrolytic–photocatalytic system.

such as methanol, methyltrimethoxysilane (MTMOS) and HCl were obtained from Merck Co. (Germany) and were used as received. The investigated photocatalyst was TiO_2 nanoparticles (Degussa P-25, Germany) having 80% anatase and 20% rutile immobilized on glass plates. It's specific surface area (BET) and particle size were 50 m^2/g and 21 nm, respectively. Multiwalled CNT was produced from Cheap Tubes Inc. (USA). It's specific surface area, outer diameters and inside diameters were 233 m^2/g, 8–15 nm and 3–5 nm, respectively.

2.2. Instruments

The experiments were performed using a DC power supply (ADAK PS 808, Iran). The solution pH was measured with a Metrohm 654 pH-meter (Switzerland). The removal of color was followed by using UV–Vis spectrophotometer (Light wave S2000, England). Before analysis of samples extracted from solutions, they were filtered with 0.2 μm membrane filter (Schleicher & Schuell, Germany). Irradiation was carried out with 6 W UV–C lamp (T5 fluorescent cool light, China), which was placed in a quartz tube inside a batch cell of 3000 mL in volume (Fig. 1b). Scanning electron microscopy (SEM) was carried out on a Philips XL 30 microscope equipped with a field-emission gun operating at 7 kV accelerating voltage. The SEM samples were previously sputter-coated with a gold film. Fig. 2 shows the SEM image of used TiO_2. As can be seen, this figure proves the nanoscale size of the used photocatalyst.

Total organic carbon (TOC) measurements were carried out by TOC analyzer of Shimadzu TOC–VCSH (North America). Nitrogen sorption analyses were obtained with a Micromeritics Tristar

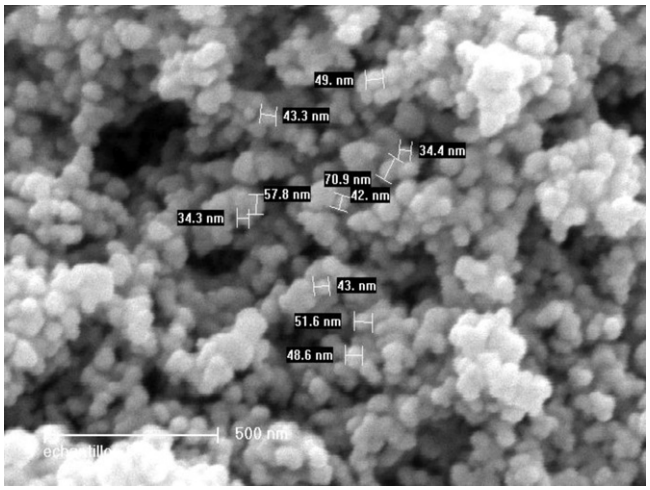

Fig. 2. Scanning electron microscopy image of TiO_2 Degussa P25.

sorptometer using standard continuous procedures at 77.15 K on calcined samples that had been degassed at 363 K for 1 h and then at 403 K under high vacuum for at least 10 h. The surface area was calculated according to the Brunauer–Emmett–Teller (BET) model [23] over a relative pressure range of 0.05–0.30. Pore diameter distribution was calculated according to the Barret–Joyne–Halenda method [23], modified by the Halsey thickness curve correction [24] on the desorption branch. BET surface area, total pore volume and pore size of TiO_2 nanoparticles were 49.7 m^2/g, 0.26 cm^3/g and 24 nm, respectively. For GC–MS analysis, an Agilent 6890 gas chromatography with a 30 m to 0.25 mm HP-5MS capillary column coupled with an Agilent 5973 mass spectrometer (Agilent Technologies, Palo Alto, CA) operating in EI mode at 70 eV was used.

2.3. Immobilization of TiO_2 nanoparticles on glass plates

TiO_2 nanoparticles were fixed on sandblasted glass plates by sol–gel dip-coating method. Organically modified silica (Ormosil) was used as hydrophobic binder. The coating solution contained 23 mL of methanol, 0.264 g of TiO_2 nanoparticles, and appropriate amount of methyltrimethoxysilane (MTMOS), which was set to achieve the desired TiO_2/Ormosil weight ratio. HCl solution (1 N) was added for hydrolysis of MTMOS. The suspension was sonicated for 15 min by a Sonoplus Ultrasonic Homogenizer HD 2200 (Burladingen, Germany). The main advantage of this kind of films is that they have good mechanical anchoring due to the chemical bonding, in comparison with films made with the dried mixture of TiO_2 and water.

2.4. Combined homogeneous photoelectro-Fenton and heterogeneous photocatalytic system

The treatment of BR46 was conducted at room temperature in an undivided, cubic tank with a capacity of about 2500 mL and performed at constant current (Fig. 1b). The CNT-PTFE electrode was selected as cathode and Pt sheets of 11.5 cm^2 area was used as anode. The distance between electrodes was about 1 cm. Fabrication and schematic diagram of CNT-PTFE electrode was explained previously [13,25]. The cathode, anode and UV lamp (placed in a quartz tube) were centered in the cell, surrounded by the TiO_2 nanoparticles immobilized on glass plates, which covered in the four side of the inner wall of the cell (see Fig. 1b). In all experiments, solutions were vigorously stirred with a magnetic bar to ensure suitable transport of reactants towards/from the electrodes. The diffusion cathode was fed with pure O_2 gas at 140 mL/min for the production of H_2O_2 from reaction (1). 2000 mL solutions of BR46 containing 0.05 M Na_2SO_4 as background electrolyte were degraded in all cases at pH 3.0. The value of pH 3.0 was chosen because several studies have shown that the optimum pH for Fenton's reaction is in the range 2.8–3.0 [13,16,26]. In order to retard the decolorization process, each 1-mL sample was mixed with 1 mL of ethanol and at the end of the reaction the remaining BR46 was determined using a spectrophotometer at λ_{max} = 530 nm and calibration curve. The color removal efficiency (CR%) was defined by the following expression:

$$\text{Color removal efficiency (CR\%)} = \left(1 - \frac{C}{C_0}\right) \times 100 \quad (12)$$

where C_0 and C are the dye concentrations at time 0 and t, respectively.

Table 1
Experimental ranges and levels of the independent test variables.

Variables	Ranges and levels				
	−2	−1	0	+1	+2
Initial Fe(III) concentration (mM) (X_1)	0.05	0.10	0.15	0.20	0.25
Initial dye concentration (mg/L) (X_2)	2	7	12	17	22
Reaction time (min) (X_3)	2	11	20	29	38
Applied current (mA) (X_4)	100	200	300	400	500

2.5. Experimental design

In the present study, central composite design (CCD), which is a widely used form of RSM was employed for the optimization of combined photoelectro-Fenton with photocatalytic process. In order to evaluate the influence of operating parameters on the decolorization efficiency of BR46, four main factors were chosen: initial Fe(III) concentration (X_1), initial dye concentration (X_2), and reaction time (X_3) and applied current (X_4). A total of 31 experiments were employed in this work, including 2^4 = 16 cube points, 7 replications at the center point and 8 axial points. Experimental data were analyzed using the Minitab 15 software. For statistical calculations, the variables X_i were coded as x_i according to the following relationship:

$$x_i = \frac{X_i - X_0}{\delta X} \quad (13)$$

where X_0 is the value of X_i at the center point and δX presents the step change [25,27,28]. The experimental ranges and the levels of the independent variables for BR46 color removal are given in Table 1.

3. Results and discussion

3.1. Decolorization and mineralization of BR46

The degradation of BR46 was carried out by using EF, PEF, UV/TiO_2 and PEF/UV/TiO_2 processes. In order to compare the above processes, 20 mg/L BR46 solutions at pH 3 have been the target in all experiments. Fig. 3 shows the removal efficiency for 20 mg/L BR46 solution under electrolysis at 100 mA and initial Fe^{3+} concentration of 0.1 mM after 60 min at room temperature (25 °C). It can be observed that the highest removal efficiency was obtained using PEF/UV/TiO_2 process. The results also showed that BR46 removal after 60 min reaction time follows the decreasing order: PEF/UV/TiO_2 > PEF > EF > UV/TiO_2. Furthermore, the dye was quickly destroyed during the first 60 min of PEF/UV/TiO_2 process, yielding 91.6% of decolorization efficiency, whereas at the same time, PEF, EF and UV/TiO_2 processes led to 83.5%, 31.7% and 12% decolorization

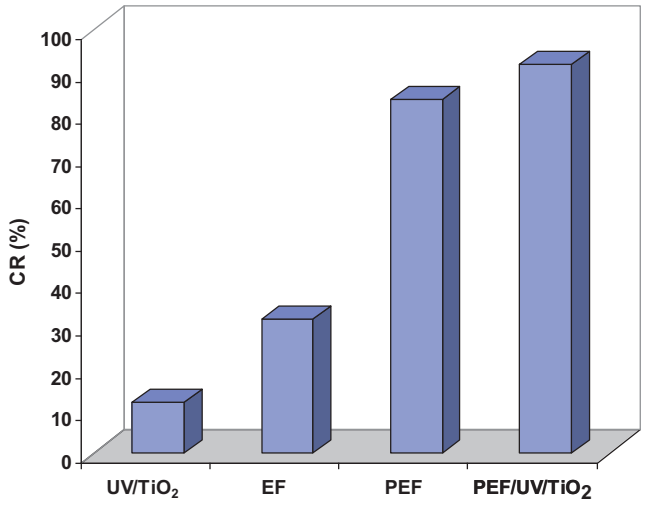

Fig. 3. Color removal efficiency (CR%) for a 20 mg/L BR46 solution at room temperature, I = 100 mA, pH 3.0, $[Na_2SO_4]$ = 0.05 M, $[Fe^{3+}]_0$ = 0.1 mM, reaction time = 60 min.

efficiency, respectively. These results indicate that combination of photoelectro-Fenton method (PEF) with photocatalytic process (UV/TiO_2) can effectively accelerate the decolorization efficiency. The efficiency of the PEF/UV/TiO_2 process to mineralize dye solution was evaluated by the TOC decay. This study was carried out with solution of pH 3.0 containing 15 mg/L of BR46 by applying 100 mA current for 6 h. A TOC abatement was observed attaining 99.2% of mineralization after 6 h of PEF/UV/TiO_2 process. TOC decay shows that the PEF/UV/TiO_2 process can effectively degrade the dye solution containing BR46.

3.2. Central composite design (CCD) model

The 4-factor CCD matrix and experimental results obtained in PEF/UV/TiO_2 process are presented in Table 2. The second-order polynomial response equation (Eq. (14)) was used to correlate the dependent and independent variables.

$$Y = b_0 + b_1x_1 + b_2x_2 + b_3x_3 + b_4x_4 + b_{12}x_1x_2 + b_{13}x_1x_3 + b_{14}x_1x_4 + b_{23}x_2x_3 + b_{24}x_2x_4 + b_{34}x_3x_4 + b_{11}x_1^2 + b_{22}x_2^2 + b_{33}x_3^2 + b_{44}x_4^2 \quad (14)$$

where Y is a response variable of decolorization efficiency. The b_i are regression coefficients for linear effects; b_{ii} are the regression coefficients for squared effects; b_{ik} are the regression coefficients for interaction effects and x_i are coded experimental levels of the variables.

Based on these results, an empirical relationship between the response and independent variables was attained and expressed by the following second-order polynomial equation:

$$Y = 54.7404 - 1.8736x_1 - 8.5718x_2 + 22.8549x_3 - 0.5604x_4 + 3.3824x_1x_2 + 1.9573x_1x_3 - 0.5392x_1x_4 - 4.0852x_2x_3 - 1.6505x_2x_4 + 1.5313x_3x_4 - 3.2163x_1^2 + 2.0539x_2^2 + 1.5344x_3^2 - 1.8855x_4^2 \quad (15)$$

The decolorization efficiencies (CR(%)) have been predicted by Eq. (15) and presented in Table 2. These results indicated good agreements between the experimental and predicted values of decolorization efficiency. The correlation coefficient (R^2) quantitatively evaluates the correlation between the experimental data and the predicted responses. The experimental results and the predicted values obtained from the model (Eq. (15)) were compared.

Table 2
The 4-factor central composite design matrix and the value of response function (CR(%)).

Run	$[Fe(III)]_0$ (mM)	$[Dye]_0$ (mg/L)	Reaction time (min)	Applied current (mA)	CR (%)	
					Experimental	Predicted
1	0.15	12	38	300	91.01	98.29
2	0.10	17	29	400	74.82	72.34
3	0.15	12	20	300	54.83	54.74
4	0.15	12	2	300	4.40	6.87
5	0.20	17	11	400	17.00	20.31
6	0.10	7	29	400	88.21	79.01
7	0.05	12	20	300	46.91	64.52
8	0.15	12	20	500	30.70	37.28
9	0.10	7	11	400	43.50	44.24
10	0.15	22	20	300	42.18	45.43
11	0.20	17	29	400	66.82	69.42
12	0.15	12	20	300	55.00	54.74
13	0.10	7	29	200	87.43	80.54
14	0.15	12	20	300	56.00	54.74
15	0.15	12	20	100	36.34	39.52
16	0.10	17	11	400	42.61	29.36
17	0.20	7	29	400	87.48	82.69
18	0.15	2	20	300	73.20	79.71
19	0.15	12	20	300	54.00	54.74
20	0.15	12	20	300	53.98	54.74
21	0.10	17	29	200	74.06	67.73
22	0.20	7	11	400	41.64	41.79
23	0.10	7	11	200	47.00	38.23
24	0.20	17	29	200	82.00	77.67
25	0.15	12	20	300	54.36	54.74
26	0.25	12	20	300	79.87	72.02
27	0.20	17	11	200	18.00	21.02
28	0.10	17	11	200	16.00	17.21
29	0.20	7	11	200	49.75	48.65
30	0.20	7	29	200	90.00	97.08
31	0.15	12	20	300	55.01	54.74

Table 3
Analysis of variance (ANOVA) for fit of decolorization efficiency from central composite design.

Source of variations	Sum of squares	Degree of freedom	Adjusted mean square	*F*-value
Regression	15830.9	14	1130.78	16.55
Residuals	1093.1	16	68.32	
Total	16924.0			

R^2 = 0.935, Adj-R^2 = 0.879.

It was found that the predicted values matched the experimental values reasonably well with R^2 = 0.9354. This implies that 93.54% of the variations for percent color removal are explained by the independent variables and this also means that the model does not explain only about 6.46% of variation. Adjusted R^2 (Adj-R^2) is also a measure of goodness of a fit, but it is more suitable for comparing models with different numbers of independent variables. It corrects R^2-value for the sample size and the number of terms in the model by using the degrees of freedom on its computations. If there are many terms in a model and not very large sample size, Adj-R^2 may be visibly smaller than R^2 [29,30]. Here, Adj-R^2 value (0.879) was very close to the corresponding R^2 value (see Table 3).

Table 3 summarizes the results of the quadratic response surface model fitting in the form of analysis of variance (ANOVA). ANOVA is required to test the significance and adequacy of the model [25,31]. ANOVA subdivides the total variation of the results in two components: variation associated with the model and variation associated with the experimental error, showing whether the variation from the model is significant or not when compared with the ones associated with residual error [25,29,32]. This comparison is performed by *F*-value, which is the ratio between the mean square of the model and the residual error. If the model is a good predictor of the experimental results, *F*-value should be greater than the tabulated value of *F*-distribution for a certain number of degrees of freedom in the model at a level of significance α. *F*-value obtained, 16.55, is clearly greater than the tabulated *F* (2.352 at 95% significance) confirming the adequacy of the model fits.

The student's *t* distribution and the corresponding values, along with the parameter estimate, are given in Table 4. The *P*-values were used as a tool to check the significance of each of the coefficients, which in turn, are necessary to understand the pattern of the mutual interactions between the test variables. The larger the magnitude of the student's *t*-test and smaller *P*-value, the more significant is the corresponding coefficient [25,31].

The Pareto analysis gives more significant information to interpret the results. In fact, this analysis calculates the percentage effect of each factor on the response, according to the following relation

Table 4
Estimated regression coefficients and corresponding *t* and *P* values from the data of central composite design experiments.

Coefficient	Parameter estimate	Standard error	*t*-Value	*P*-value
b_0	54.7404	3.124	17.522	0.000
b_1	1.8736	1.687	1.110	0.283
b_2	−8.5718	1.678	−5.080	0.000
b_3	22.8549	1.678	13.546	0.000
b_4	−0.5604	1.678	−0.332	0.744
b_{12}	3.3824	1.546	2.188	0.044
b_{13}	1.9573	1.546	1.266	0.224
b_{14}	−0.5392	1.546	−0.349	0.732
b_{23}	−4.0852	1.546	−2.643	0.018
b_{24}	−1.6505	2.066	−0.799	0.436
b_{34}	1.5313	2.066	−0.741	0.469
b_{11}	−3.2163	2.066	−1.556	0.139
b_{22}	2.0539	2.066	0.994	0.335
b_{33}	1.5344	2.066	0.743	0.469
b_{44}	−1.8855	2.066	−0.912	0.375

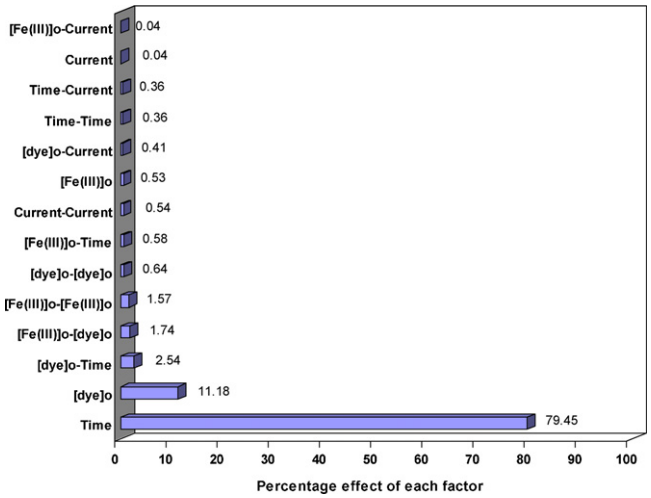

Fig. 4. Pareto graphic analysis.

[22,33]:

$$P_i = \left(\frac{b_i^2}{\sum b_i^2}\right) \times 100 \quad (i \neq 0) \tag{16}$$

Fig. 4 shows the Pareto graphic analysis. As can be seen in this figure among the variables, reaction time (b_3, 79.45%) and initial dye concentration (b_2, 11.18%) produce the main effect on decolorization efficiency.

3.3. Effect of variables as response surface and counter plots

In Fig. 5, the response surface and contour plots were developed as a function of initial dye concentration and applied current while the initial Fe(III) concentration and reaction time were kept constant at 0.15 mM and 20 min, respectively, being the central levels. As can be seen in Fig. 5, color removal efficiency decreased with increasing initial dye concentration at all applied currents. This behavior is one of the characteristics of advanced oxidation processes (AOPs). In the constant conditions of the electrolysis system (e.g. constant current, pH, etc.) certain amount of hydroxyl radicals are produced while the concentration of the dye is increased. Therefore, the amount of hydroxyl radicals is not enough to decolorize the high concentrations of the dye, then removal efficiency decreases [34]. On the other hand, decolorization efficiency of BR46 increased with increasing applied current values from 100 to 300 mA. The enhancement in decolorization efficiency with the applied current can be associated with a greater production of H_2O_2 through reaction (1). After that, the decolorization efficiency values gradually decreased and reached a steady state. Therefore the optimum current value was found to be 300 mA.

Fig. 6 shows the response surface and contour plots of the decolorization efficiency as function of reaction time and initial Fe(III) concentration. The concentration of Fe^{3+} or Fe^{2+} is a key factor in the EF processes and is a function of the cathode employed. For example, contents of 0.5–1.0 mM Fe^{2+} are optimum for carbon-PTFE GDE cathodes because of their lower ability for Fe^{2+} regeneration [16,35]. The maximum production of $OH^{\bullet}$ via Fenton's reaction takes place at the optimized Fe^{3+} or Fe^{2+} contents, since at higher catalyst concentration the oxidant generation is progressively inhibited because of the greater extent at which waste reaction 17 is given.

$$Fe(II) + OH^{\bullet} \rightarrow Fe(III) + OH^{-} \tag{17}$$

On the other hand, increasing the initial concentration of Fe^{3+} increases a brown turbidity in the solutions during the photooxida-

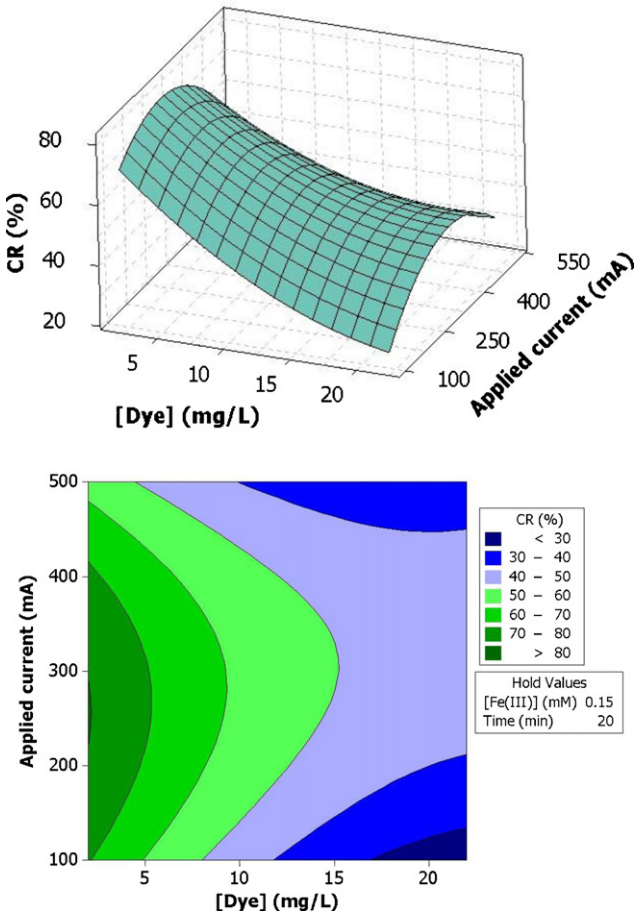

Fig. 5. The response surface plot and contour plot of the decolorization efficiency (CR%) as the function of initial dye concentration (mg/L) and applied current (mA).

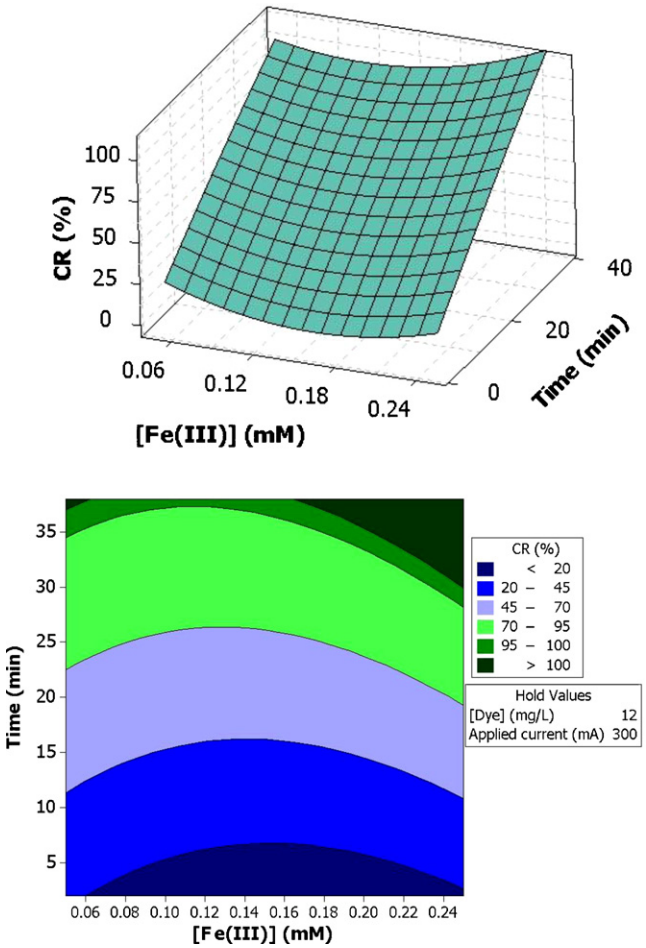

Fig. 6. The response surface plot and contour plot of the decolorization efficiency (CR%) as the function of initial Fe(III) concentration (mM) and reaction time (min).

tion process, which hinders the absorption of the UV light required for the photo-Fenton and photocatalytic processes [36]. As can be seen in Fig. 6, the decolorization efficiency decreases with an increase in the amount of Fe(III) at lower contents of Fe^{3+} and then slightly increases. This may be due to the collections of factors effect on process by Fe^{3+} content that explained above. Also, the color removal efficiency increased with increasing reaction time at all applied initial Fe^{3+} concentrations.

Fig. 7 displays the 2D and 3D plots of decolorization efficiency as a function of reaction time and initial dye concentration at a fixed initial Fe(III) concentration and applied current of 0.15 mM and 300 mA, respectively. As can be seen, an increase in initial dye concentration from 2 to 22 mg/L causes lower decolorization efficiency.

3.4. Determination of optimal conditions for decolorization of BR46

The main objective of the optimization is to determine the optimum values of variables of PEF/UV/TiO_2 process from the model obtained using experimental data. The desired goal in term of decolorization efficiency was defined as "maximize" to achieve highest treatment performance. The optimum values of the process variables for the maximum decolorization efficiency are shown in Table 5. After verifying by a further experimental test with the predicted values, the result indicated that the maximal decolorization efficiency was obtained when the values of each parameter were set at the optimum values. It implies that the strategy to optimize the decolorization conditions and to obtain the maximal decolorization efficiency by CCD for the removal of BR46 by electrochemical and photocatalytic process is successful.

3.5. Determination of dye degradation products in PEF/UV/TiO_2 process

To identify the aromatic intermediates, 2000 mL solution with 15 mg/L of BR46 was degraded at 100 mA and at room temperature (25 °C) by PEF/UV/TiO_2 process for 30 min. The electrolyzed solution was acidified at pH 1 with H_2SO_4 and saturated with Na_2SO_4, before the extraction of organic components with 30 mL of diethyl ether in three times [13]. The collected organic solution was evaporated and the remaining solid was dissolved in 100 μL of N,O-bis-(trimetylsilyl)acetamide under heating at 60 °C and stirring for 10 min. The resulting silylated products were then analyzed by GC–MS by the following temperature program: 50 °C for 4 min, 8 °C min^{-1} up to 300 °C and hold time 4 min. The temperature of the inlet, transfer line and detector was 250, 250 and

Table 5
Optimum operating conditions of the process variables.

Variable	Optimum value
Initial Fe(III) concentration (mM)	0.1
Initial dye concentration (mg/L)	15
Reaction time (min)	35
Applied current (mA)	300
Experimental CR (%)	88.89
Predicted CR (%)	90.21

Table 6
Identified aromatic by-products during degradation of BR46 by PEF/UV/TiO_2 process.

No.	Compound name	Structure	Retention time (min)	Main fragments
1	2,4-Dimethyl-2,4-dihydro-[1,2,4] triazol-3-one	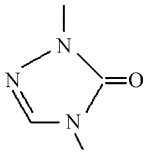	7.41	113, 84, 69, 55, 43
2	Benzenamine, N-phenylmethylene	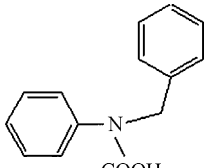	21.38	197, 182, 106, 91, 77, 51
3	Benzoic acid[a]	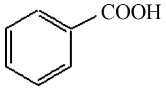	5.13	179, 135, 105, 77, 51
4	2-methyl-phenol	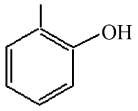	10.15	108, 90, 79, 51
5	Hydroquinone[a]	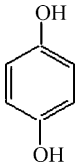	16.58	254, 239, 112, 73, 45
6	Butenedioic acid[a]	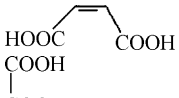	13.12	247, 147, 129 73, 45
7	Ethanedioic acid[a]		2.52	147, 131, 117, 103, 73, 59

[a] Value corresponding to the trimethylsilyl derivative.

300 °C, respectively [13,37]. The analyzed constituents were identified by matching their spectra with those recorded in the MS library (Wiley 7n). Seven compounds were successfully detected, namely 2,4-dimethyl-2,4-dihydro-[1,2,4]triazol-3-one (**1**), benzenamine, N-phenylmethylene (**2**), benzoic acid (**3**), 2-methyl-phenol (**4**), hydroquinone (**5**), butenedioic acid (**6**) and ethanedioic acid (**7**) (Table 6). It should be pointed out that, other than the compounds successfully detected, several other chromatographic peaks were also found but could not be positively identified (i.e. the match factor of the mass spectrum was below 90%). It is obvious that as soon as the aromatic ring opens a wide range of cleavage compounds are expected; unfortunately, such byproducts could not be detected due to the limitations associated with the analytical technique employed or they were not significantly accumulated in the medium. On the other hand, some of intermediates have not been identified, probably because in case of their generation, they are quickly oxidized to their derivatives. The product distribution results suggest that the degradation process is initialized by hydroxylation of BR46 to form the 2,4-dimethyl-2,4-dihydro-[1,2,4]triazol-3-one (**1**) and benzenamine, N-phenylmethylene (**2**). Afterwards, a further $OH^{\bullet}$ attack on the (**2**) bond leads to benzoic acid (**3**) and 2-methyl-phenol (**4**). Intermediate **4** is subsequently oxidized to hydroquinone (**5**). The intermediates **3** and **5** can be changed to the short-chain carboxylic acids such as butenedioic acid (**6**) by further oxidation. Oxidation of these products gives oxalic acid (**7**) that is converted directly into CO_2 and H_2O.

3.6. Electrical energy consumption

Electrical energy consumption is very important economical parameter in PEF/UV/TiO_2 process like all other photo-electrolytic processes. In this work, electrical energy consumption in the photochemical processes (E_1) was calculated according to the proposal of the Photochemistry Commission of International Union of Pure and Applied Chemistry (IUPAC) (see Eq. (18)) [38].

$$E_1 = \frac{P \times t \times 1000}{V \times 60 \times \log(C_i/C_f)} \quad (18)$$

where P is the rated power (kW) of the photochemical system, V is the volume (L) of the water in the reactor, C_i and C_f are the initial and final dye concentrations and t is the reaction time (min). So, the electrical energy (kWh/m^3) required to photochemical decolorization of 15 mg/L of the dye from 2000 mL dye solution in the optimized conditions was 1.84 kWh/m^3.

The electrical energy consumption in the electrochemical process was calculated using the commonly used Eq. (19) [39]:

$$E_2 = \frac{U \times I \times t}{V \times 3.6 \times 10^3} \quad (19)$$

where E_2 is the electrical energy in kWh/m^3, U is the cell voltage in volt (V), I is the current in ampere (A), t is the time of process per second and V is the volume (L) of the water in the reactor. The electrical energy (kWh/m^3) required to electrochemical decolorization of 15 mg/L of the dye from 2000 mL dye solution in the optimized conditions (Table 5) was 0.875 kWh/m^3. In this preliminary economic study, energy costs in electrochemical and photochemical processes are taken into account as major cost items in the calculation of the operating cost as kWh per volume (m^3) of the water in the reactor;

$$\text{Operating cost} = a(E_{\text{photochemical process}} + E_{\text{electrochemical process}}) \quad (20)$$

where $E_{\text{photochemical process}}$ (E_1) and $E_{\text{electrochemical process}}$ (E_2) are 1.84 and 0.875 kWh/m^3, respectively. 'a' is the electrical energy price in

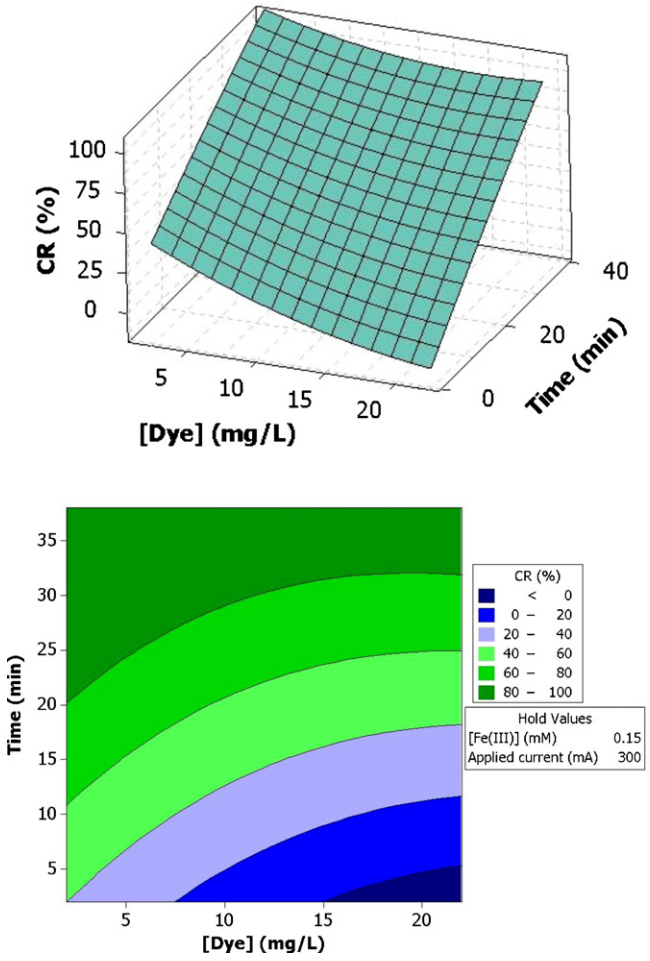

Fig. 7. The response surface plot and contour plot of the decolorization efficiency (CR%) as the function of initial dye concentration (mg/L) and reaction time (min).

Iran market in June 2010, which is equal 0.0224 US$/kWh. So, the operating cost is equal to 0.061 US$/m^3. These calculations were carried out at the optimized conditions of PEF/UV/TiO_2 process (see Table 5).

4. Conclusions

In this work, the removal of BR46 has been studied as a model dye from aqueous solutions by photocatalytic process using immobilized TiO_2 nanoparticles combined with photoelectro-Fenton process with CNT-PTFE electrode as cathode. A comparison of UV/TiO_2, EF, PEF and PEF/UV/TiO_2 for decolorization of BR46 solution was performed. The dye was quickly destroyed at the first 60 min of PEF/UV/TiO_2 process, yielding 91.6% of decolorization efficiency, whereas at the same time, PEF, EF and UV/TiO_2 processes led to 83.5%, 31.7% and 12% decolorization efficiency, respectively. Based on experimental results, an empirical relationship between the response and independent variables was attained and expressed by the second-order polynomial equation. Effect of experimental parameters on the decolorization efficiency of BR46 was established by the response surface and contour plots of the model-predicted responses. Analysis of variance showed a high coefficient of determination value (R^2 = 0.935), thus ensuring a satisfactory adjustment of the second-order regression model with the experimental data. To identify reaction by-products accompanying BR46 degradation, samples were analyzed by means of GC–MS and 7 compounds successfully detected. The operation cost for the decolorization of the dye solution containing BR46 was calculated (≈0.061 US$/m^3).

Acknowledgements

The authors thank the University of Tabriz, Iran for financial and other supports. We also sincerely thank the Water and Wastewater Company of East Azerbaijan for TOC analysis.

References

[1] H. Zollinger (Ed.), Color Chemistry. Synthesis, Properties and Applications of Organic Dyes and Pigments, second ed., VCH, 1991.
[2] A.B. Prevot, C. Baiocchi, M. Brussino, E. Pramauro, P. Savarino, V. Augugliaro, G. Marci, L. Palmisano, Environ. Sci. Technol. 35 (2001) 971–976.
[3] E. Kusvuran, O. Gulnaz, S. Irmak, O.M. Atanur, H.I. Yavuz, O. Erbatur, J. Hazard. Mater. 109 (2004) 85–93.
[4] E. Brillas, J.C. Calpe1, J. Casado, Water Res. 34 (2000) 2253–2262.
[5] Y.B. Xie, X.Z. Li, Mater. Chem. Phys. 95 (2006) 39–50.
[6] A. Wang, J. Qu, H. Liu, J. Ru, Appl. Catal. B: Environ. 84 (2008) 393–399.
[7] B. Gözmen, M.A. Oturan, N. Oturan, O. Erbatur, Environ. Sci. Technol. 37 (2003) 3716–3723.
[8] K. Hanna, S. Chiron, M.A. Oturan, Water Res. 39 (2005) 2763–2773.
[9] M. Diagne, N. Oturan, M.A. Oturan, Chemosphere 66 (2007) 841–848.
[10] E. Brillas, B. Boye, I. Sires, J.A. Garrido, R.M. Rodríguez, C. Arias, P.L. Cabot, C. Comninellis, Electrochim. Acta 49 (2004) 4487–4496.
[11] M. Skoumal, C. Arias, P.L. Cabot, F. Centellas, J.A. Garrido, R.M. Rodríguez, E. Brillas, Chemosphere 71 (2008) 1718–1729.
[12] D. Salari, A. Niaei, A.R. Khataee, M. Zarei, J. Electroanal. Chem. 629 (2009) 117–125.
[13] M. Zarei, D. Salari, A. Niaei, A.R. Khataee, Electrochim. Acta 54 (2009) 6651–6660.
[14] M.A. Oturan, J.J. Aaron, N. Oturan, J. Pinson, Pestic. Sci. 55 (1999) 558–562.
[15] Y. Sun, J.J. Pignatello, Environ. Sci. Technol. 27 (1993) 304–310.
[16] E. Brillas, I. Sirés, M.A. Oturan, Chem. Rev. 109 (2009) 6570–6631.
[17] M. Skoumal, R.M. Rodríguez, P.L. Cabot, F. Centellas, J.A. Garrido, C. Arias, E. Brillas, Electrochim. Acta 54 (2009) 2077–2085.
[18] S. Irmak, H.I. Yavuz, O. Erbatur, Appl. Catal. B 63 (2006) 243–248.
[19] T. Yates Jr., T.L. Thompson, Chem. Rev. 106 (2006) 4428–4453.
[20] A.R. Khataee, V. Vatanpour, A.R. Amani Ghadim, J. Hazard. Mater. 161 (2009) 1225–1233.
[21] A. Fujishima, T.N. Rao, D.A. Tryk, J. Photochem. Photobiol. C 1 (2000) 1–21.
[22] A. Kesraoui–Abdessalem, N. Oturan, N. Bellakhal, M. Dachraoui, M.A. Oturan, Appl. Catal. B: Environ. 78 (2008) 334–341.
[23] S. Brunauer, P.H. Emett, E. Teller, J. Am. Chem. Soc. 60 (1938) 309–319.
[24] G.D. Halsey Jr., J. Chem. Phys. 16 (1948) 931–937.
[25] M. Zarei, D. Salari, A. Niaei, A.R. Khataee, J. Hazard. Mater. 173 (2010) 544–551.
[26] C.A. Martinez-Huitle, E. Brillas, Appl. Catal. B: Environ. 87 (2009) 105–145.
[27] A.R. Khataee, M. Zarei, L. Moradkhannejhad, Desalination 258 (2010) 112–119.
[28] M.B. Kasiri, H. Aleboyeh, A. Aleboyeh, Environ. Sci. Technol. 42 (2008) 7970–7975.
[29] S.C.R. Santos, R.A.R. Boaventura, Appl. Clay Sci. 42 (2008) 137–145.
[30] G.E.P. Box, D.W. Behnken, J. Technometr. 2 (1960) 455–475.
[31] H.L. Liu, Y.R. Chiou, Chem. Eng. J. 112 (2005) 173–179.
[32] A. Aleboyeh, N. Daneshvar, M.B. Kasiri, Chem. Eng. Process. 47 (2008) 827–832.
[33] D.P. Haaland, Experimental Design in Biotechnology, Marcel Dekker, Inc., New York, Basel, 1989.
[34] N. Daneshvar, S. Aber, V. Vatanpour, M.H. Rasoulifard, J. Electroanal. Chem. 615 (2008) 165–174.
[35] I. Sirés, J.A. Garrido, R.M. Rodríguez, P.L. Cabot, F. Centellas, C. Arias, E. Brillas, J. Electrochem. Soc. 153 (2006) D1–D9.
[36] N. Daneshvar, D. Salari, A.R. Khataee, J. Photochem. Photobiol. A: Chem. 157 (2003) 111–116.
[37] C. Flox, S. Ammar, C. Arias, E. Brillas, A.V. Vargas-Zavala, R. Abdelhedi, Appl. Catal. B: Environ. 67 (2006) 93–104.
[38] J.R. Bolton, K.G. Bircger, W. Tumas, C.A. Tolman, Pure Appl. Chem. 73 (2001) 627–637.
[39] E. Vorobiev, O. Larue, C. Vu, B. Durand, Sep. Purif. Technol. 31 (2003) 177–192.